Macromolecules

Cite This: Macromolecules 2018, 51, 9562−9571

Article

pubs.acs.org/Macromolecules

Untying of Complex Knots on Stretched Polymers in Elongational Fields

Beatrice W. Soh, Alexander R. Klotz, and Patrick S. Doyle*

Department of Chemical Engineering, Massachusetts Institute of Technology, Cambridge, Massachusetts 02139, United States

Supporting Information

ABSTRACT: Knotting is a prevalent phenomenon which occurs in long polymer chains. We perform Brownian dynamics simulations and single-molecule DNA experiments to investigate knot untying in elongational fields that is induced by the knot being convected off the chain. The change in knot size as the knot moves off the chain and unties causes a change in the effective Weissenberg number, which in turn leads to a change in chain extension. Large-scale chain conformational changes are observed in both simulations and experiments for complex knots at low Weissenberg numbers (Wi). We investigate the knot untying time and untying-induced change in extension for a range of knot types and field strengths. Simulations predict a quadratic relationship between the change in extension due to knot untying and initial knot size for Wi $\geq$ 1.5. Due to the changes in chain extension as a knot unties, the untying process can be diffusion- or convection-driven.

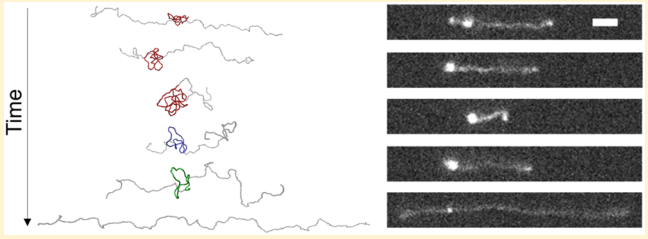

1. INTRODUCTION

Knots are common in our everyday lives, from tangled earphones to sailing knots. In the microscopic world, knots are also of important relevance, having been shown to occur naturally in DNA[1,2] and proteins.[3,4] This is not surprising; it has been theoretically proven that the knotting probability of a chain approaches unity as the chain length tends to infinity, hence knots are inevitably present in long polymer chains.[5] The probability of knot formation in polymers has been studied both computationally[6−8] and experimentally[9,10] and found to be relevant for length scales of interest. The ubiquity of knots in polymers has generated much interest in studying knots and how knots affect the physical properties of polymers.

While knots are rigorously defined only for circular chains,[11,12] long chains with free ends can contain localized, unambiguous knots, and the topologies of such chains can be closed and defined algorithmically.[13,14] Most studies on knotted polymers to date have been computational in nature and have explored a diverse range of topics, such as the equilibrium behavior of polymer knots,[15,16] translocation of knotted polymers through narrow pores,[17−21] and spontaneous knotting and unknotting in linear polymers.[22−26] More recently, researchers have demonstrated experimental methods of studying polymers with knots by introducing knots in biomolecules via optical tweezers,[27] compression in nanochannels,[28] and electric fields.[29−34] This has enabled an integrated computational and experimental approach to studying knotted polymers, with notable examples being the diffusion of knots along stretched DNA molecules under tension[27,35,36] and in elongational fields.[33,37]

From a polymer physics standpoint, the presence of knots has important consequences for overall polymer properties. Mechanically, simulations have shown that a knot reduces the strength of a polymer chain and that a knotted chain under tension usually breaks at the knot entrance.[38] Dynamically, topological constraints imposed by entanglements in polymer melts restrict chains to reptation along a tubelike region.[39−42] The effect of knots on polymer dynamics makes it interesting to study not only how molecules with knots behave but also how the knot untying process changes polymer properties. Furthermore, the knot untying process is relevant in the development of next-generation genomic technologies that are impaired by the presence of knots.[43−45]

Previous computational studies by our group have shown that knots along linear chains in elongational fields can be untied via two methods: convection off the chain beyond a critical length scale from the center of the chain at high field strengths[37] or inducing the chain to undergo a stretch-coil transition, a sharp conformational transition theoretically predicted and experimentally observed near a critical strain rate,[46,47] upon a step decrease in strain rate.[48] The former can be considered a convection-driven (field-driven) knot untying regime and the latter a diffusion-driven regime. There exists, however, an intermediate regime of knot untying along stretched chains in which single-molecule experiments mostly take place.[33] In this study, we use Brownian dynamics simulations to systematically study the dynamics of knot untying in elongational fields that is induced by the knot being convected off the chain at intermediate field strengths. The knot untying process is amenable to study by simulations because of the ability to

Received: August 31, 2018
Revised: November 6, 2018
Published: November 20, 2018

Downloaded via MASSACHUSETTS INST OF TECHNOLOGY on December 11, 2018 at 23:39:08 (UTC).
See https://pubs.acs.org/sharingguidelines for options on how to legitimately share published articles.

© 2018 American Chemical Society

DOI: 10.1021/acs.macromol.8b01879
Macromolecules 2018, 51, 9562−9571

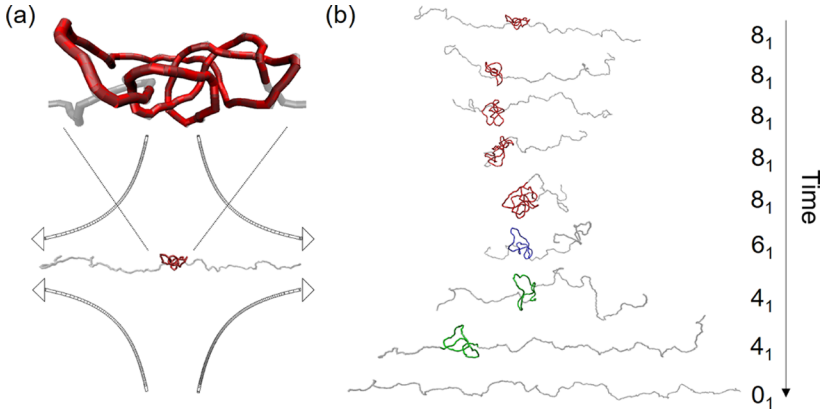

Figure 1. (a) Schematic of simulation setup: knotted (red) and unknotted (gray) regions of DNA extended in an elongational field. (b) Simulation snapshots of an initially centered 8_1 knot being convected off a chain and untying in multiple steps at field strength Wi = 1.25. The 8_1 knot (red) partially unties to a 6_1 knot (blue) and 4_1 knot (green) before completely untying.

simulate specific knot types and examine the dynamics with high temporal and spatial resolution. We complement our simulations with single-molecule DNA experiments to demonstrate that the simulations predict a realistic phenomenon. This work focuses on the chain dynamics as the knot unties and considers a range of complex knot topologies and field strengths, which differs from previous studies that examined the knot translation mechanism[37] and demonstrated changes in chain conformation during knot untying for simple knots.[48] We subject molecules with a range of knot types to elongational fields of different Weissenberg numbers (Wi) and observe the transient dynamics of the chain during and after knot convection off the chain. Specifically, we focus on the change in chain extension induced by knot untying and the time required for a knot to completely untie. We use scaling analysis and empirical results to show that simulations predict a quadratic relationship between the untying-induced change in extension and initial knot size for Wi $\geq$ 1.5. While a knot is initially convected off the chain by the elongational field, the untying process can be diffusion- or convection-driven depending on the knot topology and field strength.

2. METHODS

2.1. DNA Model. We used a Brownian dynamics approach to simulate double-stranded DNA, which has been parametrized extensively in the literature.[35,49−51] The choice of DNA model for our simulations is motivated by the prevalent use of DNA as a model polymer in single-molecule experiments. The DNA molecule is modeled as a linear bead−rod chain of N = 300 beads of diameter b at positions $\mathbf{r}_i$, connected by $N-1$ rigid rods of length l = 10 nm (5 bonds per persistence length l_p = 50 nm). To derive the governing stochastic differential equation, we consider the form of all forces acting on the system: bending, electrostatic, excluded volume, hydrodynamic, constraint, and Brownian.

The semiflexible nature of DNA is enforced by accounting for bending energy, given by

$$E^b = \frac{g}{2}\sum_{i=1}^{N-2}\theta_i^2 \tag{1}$$

where θ_i is the bending angle between bond i and bond i+1 and g = 4.81 k_bT is chosen to set l_p = 50 nm when l = 10 nm.[35] Expressions for the resulting bending force are given in Allison et al.[49] A screened Debye−Huckel potential is used to model the long-range electrostatics of DNA−DNA interactions and is specified by

$$E^e = \frac{\nu^2 l^2}{D}\sum_{i,j}^{N}\frac{\exp(-\kappa r_{ij})}{r_{ij}} \tag{2}$$

where ν = 2.43 e/nm is the effective linear charge density of DNA at an ionic strength of 10 mM, D is the dielectric constant of water, κ^{-1} is the Debye length, and r_{ij} is the distance between beads i and j. At an ionic strength of 10 mM, DNA has an effective width of ∼16 nm and a Debye length of ∼3 nm.[10,52] The excluded volume potential, leading to short-range repulsion interactions between beads, is enforced to prevent self-crossings and is determined as

$$E^{ev} = -\sum_{i,j}^{N}\mu r_{ij} \quad \text{if } r_{ij} < b \tag{3}$$

where μ = 35 pN has been shown to result in a low frequency of chain crossings[35,53] and b = 2 nm is the bead diameter. The electrostatic and excluded volume forces ($\mathbf{F}^e$ and $\mathbf{F}^{ev}$) can be obtained by taking the derivatives of the respective energies. In this work, hydrodynamic interactions between chain segments are neglected, so the drag force on the ith bead is given by

$$\mathbf{F}_i^d = \zeta\left(\mathbf{u}(\mathbf{r_i}) - \frac{d\mathbf{r_i}}{dt}\right) \tag{4}$$

where ζ is the drag coefficient of a single bead and $\mathbf{u}(\mathbf{r_i})$ is the undisturbed solvent velocity. The constraint force is described by

$$\mathbf{F}_i^c = T_i\mathbf{b}_i - T_{i-1}\mathbf{b}_{i-1} \tag{5}$$

where $\mathbf{b}_i$ is the unit vector of bond i and T_n is the tension in rod i that enforces the constraint of constant bond length. The Brownian forces are random forces that satisfy the fluctuation−dissipation theorem, such that

$$\langle\mathbf{F}_i^{br}(t)\rangle = 0 \text{ and } \langle\mathbf{F}_i^{br}(t)\mathbf{F}_j^{br}(t)\rangle = \frac{2k_bT\zeta\mathbf{I}\delta_{ij}}{\Delta t} \tag{6}$$

where δ_{ij} is the Kronecker delta, $\mathbf{I}$ is the identity matrix, and Δt is the simulation time step.

2.2. Numerical Simulation. With the neglect of chain inertia, the forces on the beads sum to zero and results in the Langevin equation that describes the motion of each bead:

$$\frac{d\mathbf{r_i}}{dt} = \mathbf{u}(\mathbf{r_i}) + \frac{1}{\zeta}(\mathbf{F}^b + \mathbf{F}^e + \mathbf{F}^{ev} + \mathbf{F}^c + \mathbf{F}^{br}) \tag{7}$$

To evaluate the bead positions at each time step, we performed a predictor-corrector scheme described in detail by Liu et al.[54] and used a time step $\Delta t = 5\times10^{-3}\tau_d$, where $\tau_d = l^2\zeta/k_bT$ is the characteristic rod diffusion time. Enforcing the rigid rod constraints gives rise to a system of nonlinear equations for the rod tensions T_i, which we solved for using Newton's method.[55]

DOI: 10.1021/acs.macromol.8b01879
Macromolecules 2018, 51, 9562−9571

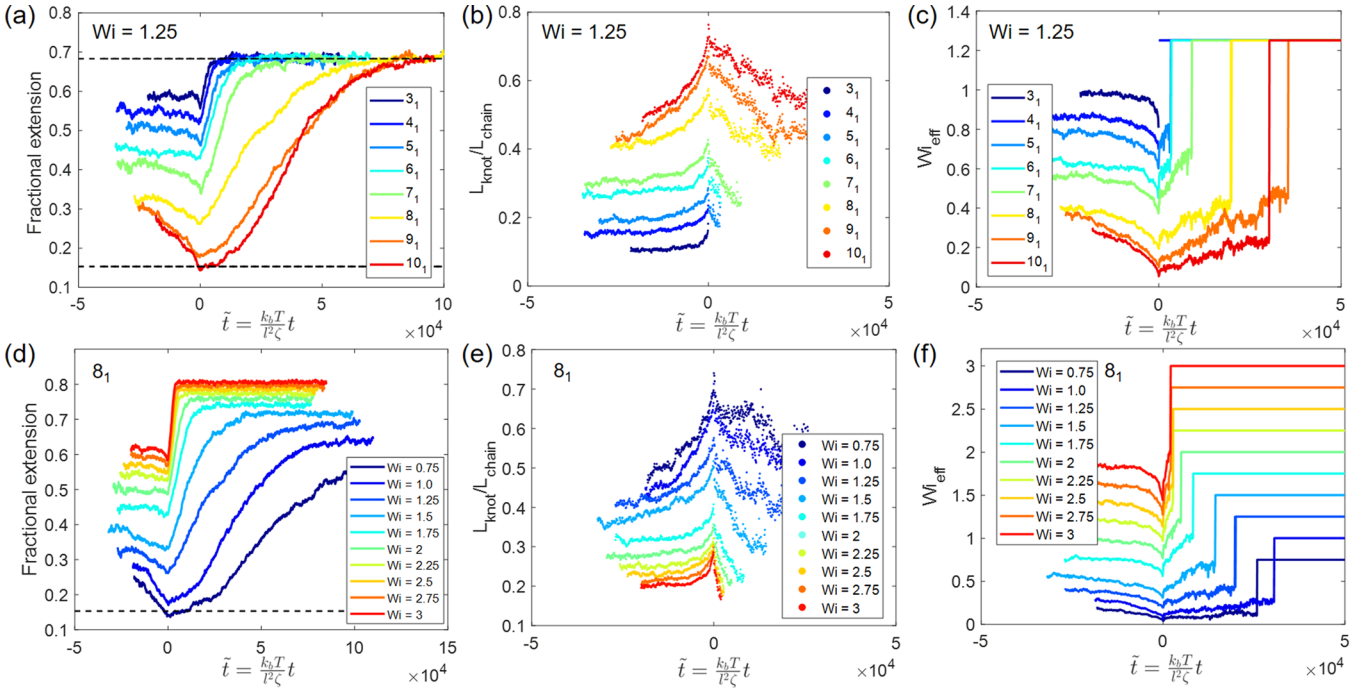

Figure 2. Simulation results showing (a) chain extension, (b) knot size, and (c) Wi_{eff} as a function of time as the initially centered knot convects off the chain and unties for chains with different knot types in an elongational field (Wi = 1.25). Curves are averaged over 50 simulation runs. The time axis has been shifted such that the knot first reaches the end of the chain at $\tilde{t} = 0$. The dotted lines in (a) represent the steady-state chain extension for the unknotted chain at Wi = 1.25 (top) and Wi = 0 (bottom). (d) Chain extension, (e) knot size, and (f) Wi_{eff} as a function of time as the initially centered 8_1 knot convects off the chain and unties for chains in elongational fields of varying strengths. Curves are averaged over 50 simulation runs. The time axis has been shifted such that the knot first reaches the end of the chain at $\tilde{t} = 0$. The dotted line in (d) represents the equilibrium unknotted chain extension.

In the simulations, we tied a knot into the center of the polymer chain and stretched the knotted chain in a planar elongational field of the form $\mathbf{u}(\mathbf{r}_i) = \dot{\epsilon}(\hat{\mathbf{x}}-\hat{\mathbf{y}})\cdot\mathbf{r}_i$, where $\dot{\epsilon}$ is the strain rate and $\hat{\mathbf{x}}$ and $\hat{\mathbf{y}}$ are unit vectors parallel to the x and y axes, respectively (Figure 1a). The response of molecules in elongational fields is characterized by the Weissenberg number $Wi = \dot{\epsilon}\tau$, where τ is the longest relaxation time of the polymer molecule and is determined by fitting the last 30% extension of an initially stretched chain to a single-exponential decay. For a given set of simulation parameters, the knotted chains were equilibrated at the simulation conditions for $10^4\tau_d$. During equilibration, the positions of the knots were held at the center of the chain via reptation moves, in which a polymer segment would be cut off from one end of the chain and appended to the other end. We ran the simulations for $2 \times 10^7\tau_d$. Figure 1b shows snapshots from a representative simulation run, in which the initially centered knot is convected to the end of the chain and proceeds to untie in multiple steps. The knotted region was colored based on the topology identified algorithmically, as described in the next section.

2.3. Knot Detection. Mathematically, knots are well-defined only in closed, circular chains. To determine the topology of open chains, we first closed the chains into a ring with an auxiliary arc by implementing the minimally interfering closure scheme, in which the auxiliary arc is constructed to minimize additional entanglement that may be introduced during chain closure.[13,14] The chain topology was then determined by projecting the chain onto a plane parallel to the extension axis, identifying all chain crossings and calculating the Alexander polynomial.[56] The knot position and boundaries of the knot were identified by determining the smallest subset of the chain that retained the topology of the whole chain via calculation of the Alexander polynomial. To ensure that the knot boundaries identified were not biased by the choice of plane projection, we repeated the procedure over many projections along the extension axis and selected the projection that resulted in the median knot size. Identifying the left and right boundaries of the knot allowed for the computation of the number of beads in the knotted region and the central bead of the knot. The knot detection algorithm is also detailed in previous publications from our group[21,37,48,57] In this work, knot position is defined as the projected distance between the central bead of the knotted region and the first bead on the chain along the primary extension of the field, and knot size refers to the fractional contour stored within the knot.

2.4. Experimental Method. The single-molecule DNA experiments follow the general protocol in previous work from our group (see the Supporting Information for detailed experimental method).[32,34,48] Briefly, a solution of fluorescently stained, T4 DNA (stained contour = 77 μm) is loaded in a 2 μm tall cross-slot channel with electrodes at the inlets and outlets. The longest relaxation time of T4 DNA was obtained by fitting the last 30% extension of an initially stretched chain to a single-exponential decay and determined to be $\tau = 2.1$ s. We first pulsed a square wave electric field of ~1000 V/cm for ~1s at 10 Hz in the center of the channel to collapse the DNA into a compact globule, which likely contains one or more knots in its interior.[29,31−34] We next applied a constant voltage drop to generate a planar elongational field within the channel. We stretched the DNA at the field's stagnation point and recorded its dynamics over time. The knots appear as bright regions of excess fluorescence on the extended chain. Although we do not know the topologies of the knots generated, we can infer information about knot complexity from the knot size, as determined from the integrated fluorescence intensity in the knotted portion of the chain.[32,34] We note that the protocol for inducing knots in our experiments does not allow for precise control over knot type and size, hence we are unable to gather a large ensemble of molecules with the same knot type or size and perform ensemble averaging.

3. RESULTS

3.1. Characteristics of Knot Untying Process. As a knot convects off the chain in an elongational field, the knot grows in size and the chain undergoes a decrease in extension (Figure 1b). When the knot reaches the end of the chain, depending on the knot type and orientation, it can untie either completely or

DOI: 10.1021/acs.macromol.8b01879
Macromolecules 2018, 51, 9562−9571

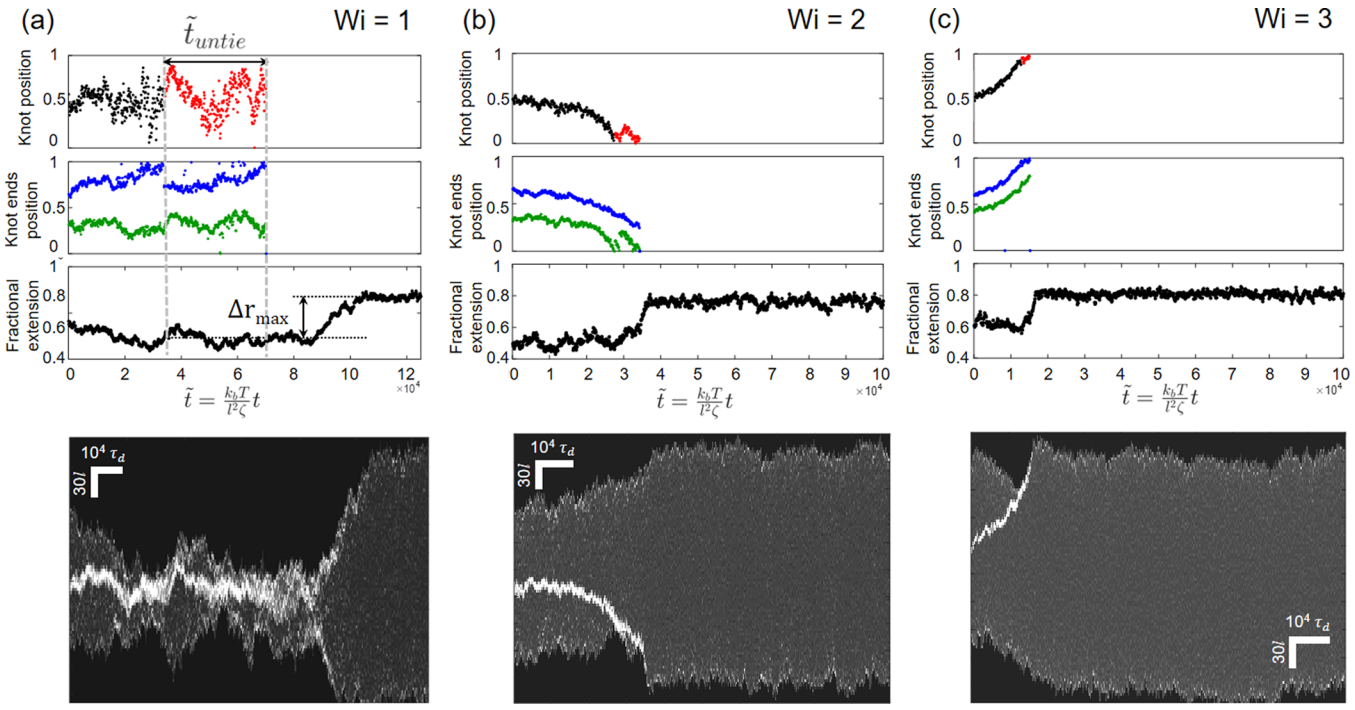

Figure 3. Individual simulation trajectories at different Wi. Knot position, knot ends position, fractional extension, and kymograph of chains with an initially centered 8_1 knot from representative simulation trajectories in elongational fields (a) Wi = 1, (b) Wi = 2, and (c) Wi = 3. The black and red points for knot position represent the points before and after the 8_1 knot first reaches the chain end, respectively. The green and blue points for knot ends position refer to the left and right boundaries of the knot, respectively. The kymographs plot 1D chain projections vs time.

partially into a less complex knot, resulting in a change in the calculated Alexander polynomial. See the Supporting Information for representative simulation movies and the Supporting Information for schematics of knot types studied. We plot in Figure 2 (panels a and b) the chain extension and knot size for a range of knot types convecting off a chain in an elongational field of strength Wi = 1.25. In Figure 2 (panels d and e), we show plots of chain extension and knot size for chains with an 8_1 knot in elongational fields from Wi = 0.75 to Wi = 3 as the knot convects off the chain and unties. All curves are averaged over 50 simulation runs and the time axis is shifted such that the knot reaches the chain end at $\tilde{t} = t/\tau_d = 0$. Chain extension is determined as the projected distance along the primary axis of extension of the field. As seen from Figure 2 (panels a and d), for all knot types and all Wi studied, the chain extension decreases as the knot convects off the chain, reaches a minimum when the knot reaches the chain end, and subsequently stretches back to the steady-state chain extension for the unknotted chain. Figure 2 (panels b and e) shows the concurrent growth in knot size as the knot is convected off the chain, with the knot size attaining a maximum when the knot reaches the chain end and decreasing as the knot partially unties. More complex knots and lower Wi give rise to larger changes in knot size and chain extension during the knot untying process. Furthermore, more complex knots require more steps to untie, hence the chains take a longer time to stretch to the unknot steady-state extension compared to simpler knots at the same Wi.

We can understand the evolution in chain extension during the knot untying process by considering the effective Weissenberg number $\mathrm{Wi}_{\mathrm{eff}}$, defined for the Rouse regime as[34,48]

$$\mathrm{Wi}_{\mathrm{eff}} = \mathrm{Wi}\left(1 - \frac{L_{\mathrm{knot}}}{L_{\mathrm{chain}}}\right)^{1+2\nu} \tag{8}$$

where $L_{\mathrm{knot}}/L_{\mathrm{chain}}$ is the fractional knot size and $\nu = 0.588$ is the excluded volume Flory exponent.[58] Figure 2 (panels c and f) shows $\mathrm{Wi}_{\mathrm{eff}}$ as a function of time during the knot untying process. As an initially centered knot convects off the chain in an elongational field, the decrease in tension along the chain results in an increase in knot size. This leads to a decrease in $\mathrm{Wi}_{\mathrm{eff}}$ and, consequently, a decrease in chain extension. When the knot reaches the chain end, it begins to untie. Depending on the knot topology and orientation, the knot can untie in either one or multiple steps. As the knot unties, the knot size decreases, leading to an increase in $\mathrm{Wi}_{\mathrm{eff}}$ and, subsequently, an increase in chain extension. After the knot fully unties, $\mathrm{Wi}_{\mathrm{eff}} = \mathrm{Wi}$ and the chain stretches to the steady-state extension for the unknotted chain. Such dynamics are not observed in knotted chains that untie while held at constant tension (see Figure S3), affirming that this phenomenon is attributable to a coupling with the elongational field and not purely caused by end effects.

For the more complex knots studied at Wi = 1.25, such as the 9_1 and 10_1 knots, the knot size is large enough to result in $\mathrm{Wi}_{\mathrm{eff}} < 0.5$ throughout the knot untying process, which leads to the large deviation in chain extension from the unknot steady-state extension. Similarly, for the smaller Wi investigated, such as Wi = 0.75 and Wi = 1.0, the resulting size of the 8_1 knot leads to $\mathrm{Wi}_{\mathrm{eff}} < 0.5$ throughout the knot untying process, hence the chain undergoes a significant change in extension as the knot unties. Essentially, for large knots and low Wi, the resulting knot size is sufficient to bring the molecule through the coil−stretch transition as the knot unties, hence giving rise to large, transient changes in chain conformation during the untying process.

To gain more insight into the untying process, we consider individual chain trajectories. Figure 3 shows simulated traces of molecules with an initially centered 8_1 knot convecting off the chain and untying in elongational fields of varying strengths. The knot position is defined as the projected distance between the

DOI: 10.1021/acs.macromol.8b01879
Macromolecules 2018, 51, 9562−9571

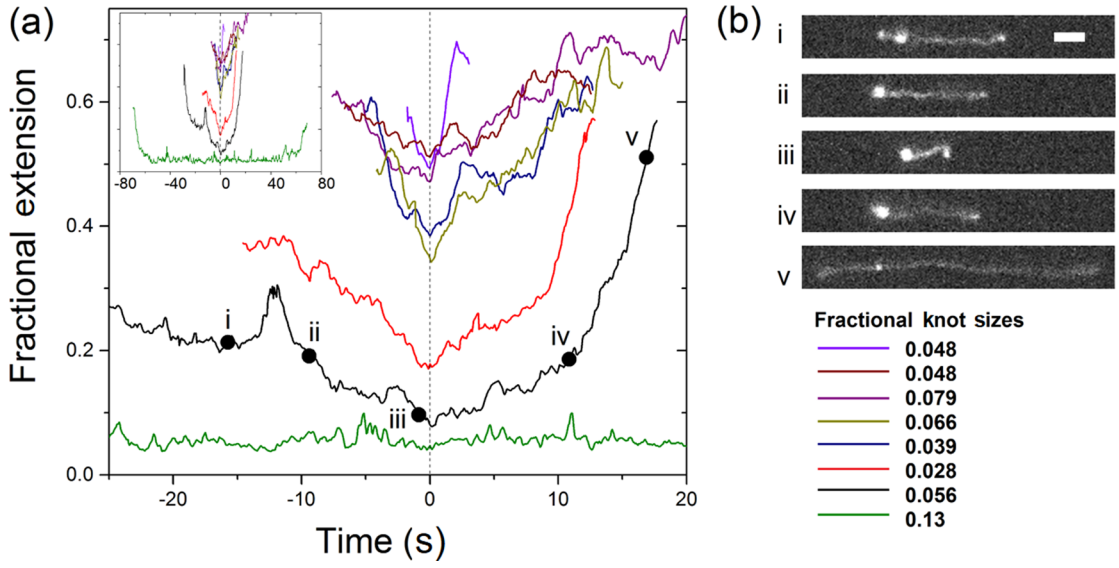

Figure 4. Experimental results at a fixed Wi. (a) Chain extension over time of several DNA molecules stretched in an elongational field (Wi = 1.75) as the knots untie. The fractional knot sizes of the molecules, measured as the integrated fluorescence intensity of the knot when the chain was stretched at Wi ∼ 3 divided by the integrated fluorescence intensity of the entire chain, are reported in the legend. The time scale of each trace is centered at the point of minimum extension. The inset shows the same data at a wider range of times. (b) Five representative images of the molecule represented by the black time trace. The scale bar is 5 μm.

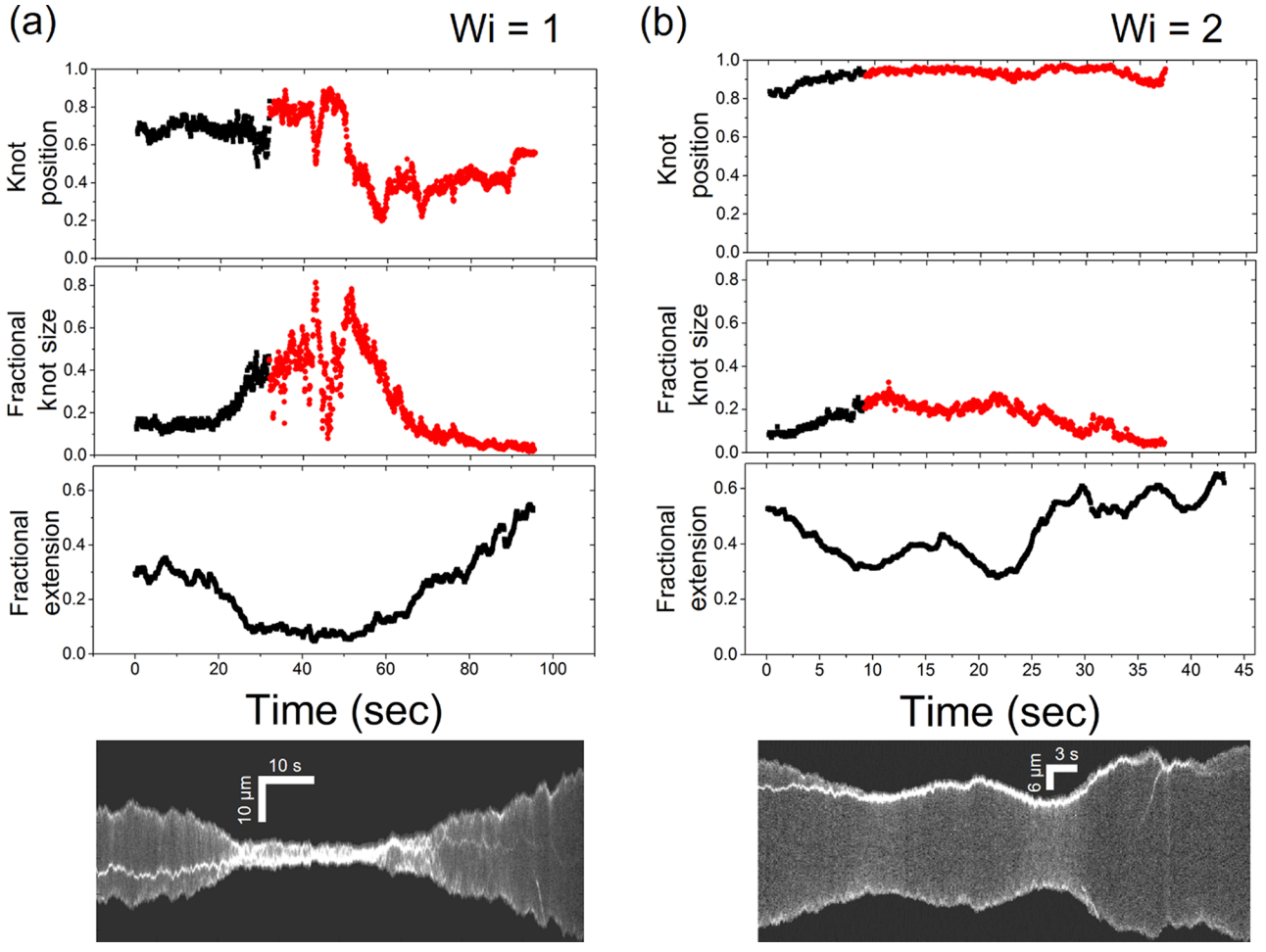

Figure 5. Experimentally measured knot position, fractional knot size, fractional extension, and kymograph of chains during the untying process in elongational fields (a) Wi = 1 and (b) Wi = 2. The fractional knot sizes, estimated as the integrated intensity of the knot when the chain is stretched at Wi ∼ 3, are 0.045 and 0.05 for (a) and (b), respectively. The black and red points for knot position and knot size represent the points before and after the knot first becomes indistinguishable from the chain end, respectively. The kymographs plot 1D chain projections vs time.

DOI: 10.1021/acs.macromol.8b01879
Macromolecules 2018, 51, 9562−9571

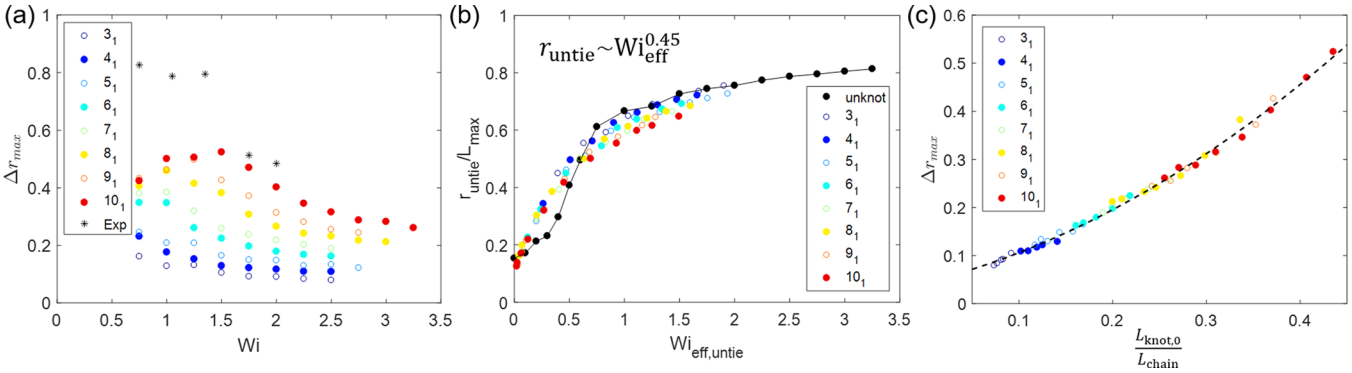

Figure 6. (a) Plot of Δr_{max} as a function of Wi for different knot types. Each point is averaged over 50 simulation runs or 5−10 experimental runs. (b) Normalized extension-Wi curves at $\tilde{t} = 0$ for different knot types. The black line is drawn to guide the eyes. (c) Plot of Δr_{max} as a function of initial knot size (fractional) for different knot types, Wi ≥ 1.5. The dotted line represents the quadratic curve of best fit to the simulation results, given by $y = 1.36x^2 + 0.49x + 0.04$. See the Supporting Information for plots with error bars.

central bead of the knotted region and the first bead on the chain along the primary extension of the field, with a knot position of zero indicating that the knot is at the left end of the molecule. The knot ends positions are the positions of the beads at the left and right boundaries of the knot.

From Figure 3, we observe distinct qualitative differences in the trajectories of molecules subjected to different field strengths. First, as expected based on Figure 2d, the molecule at Wi = 1 undergoes a more significant change in extension during the knot untying process compared to the molecules at Wi = 2 and Wi = 3. Second, the knot appears to move around the chain in a diffusive manner at low Wi, whereas it is clearly convected off the chain in a certain direction at high Wi. This can be attributed to the chain being in the coiled versus elongated state at low versus high Wi, which is determined by Wi_{eff} and can be visualized from the kymographs, and suggests that the knot untying process can be diffusion- or convection-driven. Third, at low Wi, the knot tends to move inward upon partial untying, while at high Wi, the knot tends to stay near the chain end as it unties. This can be seen clearly from the plot of knot ends position, with the right boundary of the knot moving inward upon the knot reaching the chain end at Wi = 1. The knot tends to move inward after partially untying at low Wi due to the contour released from the relatively large knot upon the first untying step. For the partial knot to fully untie, it then has to move to the chain end again, hence it is unsurprising that the same knot takes a longer time to untie at low Wi.

3.2. Experimental Observations. In this section, we present individual experimental trajectories of knotted molecules that undergo the unknotting process when stretched in elongational fields. We highlight the difficulty in gathering large ensembles of molecules with the same knot type and size experimentally, hence experimental observations are based on trajectories of chains with various knot types and sizes. Figure 4 displays experimental results for the change in extension of several DNA molecules with a range of knot sizes as the knot is convected off the chain in an elongational field Wi = 1.75. Each trace represents one molecule and the time axis has been shifted such that the chain is at minimum extension at $t = 0$. The fractional knot sizes of the molecules are determined as the integrated fluorescence intensity of the knot when the chain was stretched at Wi ∼ 3 divided by the total integrated fluorescence intensity of the chain. As seen from Figure 4a, large-scale changes in extension during the knot untying process are also observed experimentally. The nonmonotonic trend in extent of conformational change with respect to knot size is likely due to the lack of ensemble averaging for experimental results (see the Supporting Information for examples of variations in individual simulated trajectories for the same and different knot types at a constant Wi). It is worth noting that the knots observed experimentally can remain in a partially untied state for long periods of time. For example, the molecule represented by the green trace in Figure 4a, which we infer to be the most complex topologically based on knot size, remains in a partially untied, coiled state for ∼80τ (τ = 2.1 s). The experimental images in Figure 4b highlight the significant conformational changes observed in a DNA molecule as the knot is convected off the chain and partially unties into a smaller knot and qualitatively resemble the simulation snapshots shown in Figure 1b.

Next, we consider individual experimental unknotting trajectories at different Wi (Figure 5). At Wi = 2, the molecule experiences fluctuations in extension as the knot convects off the chain and partially unties, although not as drastic as the changes observed at a lower Wi. At Wi = 1, the continually increasing knot size and resulting Wi_{eff} leads to the chain undergoing a stretch-coil transition as the knot moves off the chain, followed by a coil−stretch transition after the knot partially unties. The knot also appears to diffuse about the chain after partially untying at Wi = 1, during which the molecule is in a coiled state, whereas the knot motion looks to be more directed at a higher Wi, with the knot remaining close to the chain end during the untying process. We observe qualitatively similar features between the individual experimental and simulated (Figure 3) unknotting trajectories.

On the basis of the individual molecule trajectories, we can define two quantitative metrics: untying time and untying-induced change in extension. The untying time, $\tilde{t}_{untie}$, is defined as the time taken for a knot to completely untie and is measured as the time between when the calculated Alexander polynomial first changes (when the knot first reaches the chain end) and when the Alexander polynomial is equal to 1 for the unknot (Figure 3a). By definition, the simplest knot types 3_1 and 4_1, which are typically studied in other unknotting studies, have an untying time of zero as these knots untie in one step. The untying-induced change in extension, Δr_{max}, is evaluated as the difference in extension when the Alexander polynomial first changes and the steady-state extension after fully untying (Figure 3a). Due to the difficulty in determining when the knot first reaches the chain end in experiments, we use the point of minimum chain extension in place of when the knot first reaches

DOI: 10.1021/acs.macromol.8b01879
Macromolecules 2018, 51, 9562−9571

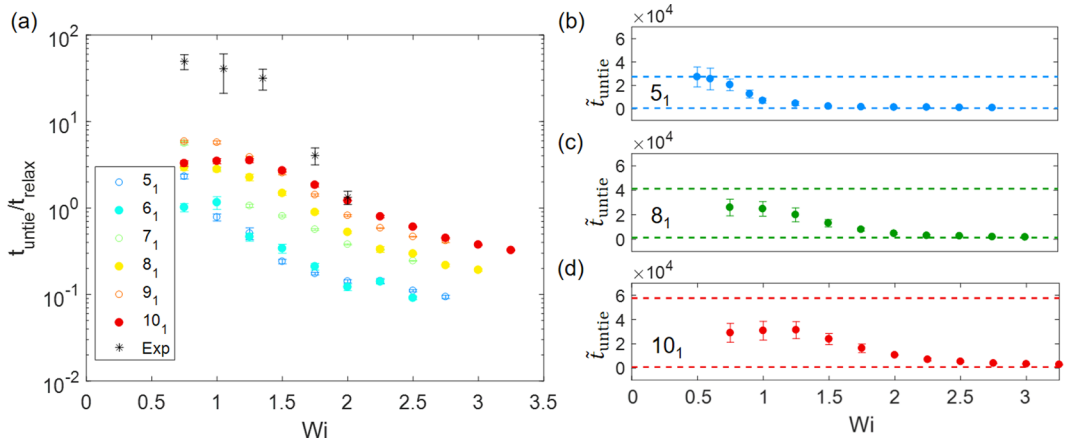

Figure 7. (a) Untying time scaled by chain relaxation time as a function of Wi for simulated chains with different knot types and experimental data. Each point is averaged over 50 simulation runs or 5−10 experimental runs. Untying time $\tilde{t}_{untie}$ as a function of Wi for chains with a (b) 5_1, (c) 8_1, and (d) 10_1 knot. The dashed lines are the untying times for chains with the same knot type held under constant tension $\tilde{F} = Fl/k_bT = 1$ (top) and in an elongational field without Brownian motion (bottom). Error bars represent 95% confidence interval (see the Supporting Information for calculation).

the chain end in obtaining t_{untie} and Δr_{max} from experimental data. If the knot partially unties into a smaller knot, t_{untie} is the time between the point of minimum chain extension and when the smaller knot is distinguishable from the chain ends; if the knot appears to untie completely, t_{untie} is the time between the point of minimum chain extension and when the intensity of both chain ends are comparable.

3.3. Untying-Induced Change in Chain Extension. Figure 6a plots Δr_{max} as a function of Wi for a range of simulated knot types and experimental data (see the Supporting Information for Figure 6 with error bars). In general, the more complex the knot type and the lower the Wi, the larger the change in chain extension induced by knot untying, in agreement with both the averaged and individual trajectories presented in Figures 2−5. For the most complex knots studied, we observe a nonmonotonic trend in Δr_{max}. This is a consequence of there being a lower limit to the extension a molecule can attain when the knot reaches the chain end (knotted chain radius of gyration), which the chains with larger knots are likely to have reached within the range of Wi studied. Although the experimentally generated knot topologies are not known, we can average data for the same Wi and observe that the trend for the experimental data points is consistent with that from the simulations. We note that the values of Δr_{max} measured experimentally are much larger than those determined from simulations, which suggests that the knots generated by an electrodydrodynamic instability in our experimental setup are much more complex and contain more contour than the 10_1 knot (knot contour ≈1 μm at Wi = 3), in agreement with findings from our previous work.[32]

To understand the physics behind these observations, we look at what determines Δr_{max}, determined as the difference between the steady-state unknot extension and extension when the knot first reaches the chain end:

$$\Delta r_{max} = r(\mathrm{Wi}) - r_{untie}(\mathrm{Wi}_{eff,untie}) = r(\mathrm{Wi}) - r_{untie}(\mathrm{Wi}, L_{knot}^{untie}) \quad (9)$$

where $r(\mathrm{Wi})$ is the steady-state extension after the knot fully unties, and r_{untie}, $\mathrm{Wi}_{eff,untie}$, and L_{knot}^{untie} are the chain extension, Wi_{eff}, and knot size, respectively, when the knot first reaches the chain end. Above a certain Wi, the steady-state chain extension does not vary much as a function of Wi. If we assume $r(\mathrm{Wi})$ to be approximately constant, then Δr_{max} is driven by r_{untie}, which is in turn dependent on $\mathrm{Wi}_{eff,untie}$, or Wi and L_{knot}^{untie}.

In Figure 6b, we plot r_{untie} normalized by L_{max} as a function of $\mathrm{Wi}_{eff,untie}$, where L_{max} is the maximum extension that the knotted molecule can achieve. Previous publications from our group show that rescaling extension by L_{max} and Wi by Wi_{eff} leads to the collapse of extension-Wi curves for knotted molecules onto that for unknotted molecules.[34,48] As shown in Figure 6b, the normalized extension-Wi curves for the knotted molecules are shifted relative to that for the unknot, from which we can infer that r_{untie} is not determined by steady-state dynamics. This is to be expected, given that knot untying is a dynamic process. We can empirically fit a power law to the normalized extension-Wi curves for the knotted molecules and determine the best fit curve to be $r_{untie} \sim \mathrm{Wi}_{eff}^{0.45}$.

Therefore, assuming Wi to be large enough to approximate $r(\mathrm{Wi})$ as constant, say Wi ≥ 1.5, we have

$$\Delta r_{max} \sim r_{untie} \sim \mathrm{Wi}_{eff}^{0.45} \sim \left(\frac{L_{knot}^{untie}}{L_{chain}}\right)^{0.45(1+2\nu)} \approx \frac{L_{knot}^{untie}}{L_{chain}} \quad (10)$$

Given that $L_{knot}^{untie}/L_{chain}$ is subject to end effects and difficult to measure experimentally, we choose to investigate Δr_{max} as a function of the initial knot size $L_{knot,0}/L_{chain}$, which is a more well-defined metric. We find empirically that simulations predict a quadratic relationship between $L_{knot,0}/L_{chain}$ and $L_{knot}^{untie}/L_{chain}$. Thus, we expect a quadratic relationship between Δr_{max} and $L_{knot,0}/L_{chain}$. We plot Δr_{max} as a function of $L_{knot,0}/L_{chain}$ for all knot types at Wi ≥ 1.5 in Figure 6c and indeed observe the collapse of simulation results onto a master quadratic curve. We highlight that the existence of a universal curve shows that the untying-induced change in extension is determined solely by the initial knot size and is not a function of Wi or knot type. The quadratic relationship between Δr_{max} and $L_{knot,0}/L_{chain}$ explains why we generally observe two chains with slightly different initial knot sizes undergo noticeably different conformational changes as the knot unties, such as the 8_1 knot at Wi = 1.5 and Wi = 1.75 depicted in Figure 2 (panels d and e, respectively). See the Supporting Information for more details on Δr_{max} scaling, determination of L_{max}, empirical fits to simulation results, and testing of significance of the quadratic regression model.

DOI: 10.1021/acs.macromol.8b01879
Macromolecules 2018, 51, 9562−9571

3.4. Knot Untying Time. Figure 7a shows the untying time as a function of Wi for a range of simulated knot types and experimental data. Generally, the more complex the knot type and the lower the Wi, the longer it takes for the knot to untie. The experimental trend for untying time agrees with that from the simulations, which supports that the model used in our simulations is sufficient for capturing the physics of the untying process despite being simplistic. The experimentally measured untying times relative to chain relaxation time are an order of magnitude larger than those determined from simulations at a given Wi, again suggesting that the knots we generate experimentally have much more complex topologies than the 10_1 knot. As seen from Figure 7a, the untying times for all knot types appear to plateau at small Wi.

To further investigate the knot untying times, we plot in Figure 7 (panels b−d) the untying times for a 5_1, 8_1, and 10_1 knot as a function of Wi. For reference, we also plot the upper and lower bounds for untying times of each knot, where the upper bound is the untying time for the knotted chain held under constant tension and the lower bound is the untying time for the knotted chain in an elongational field with no Brownian motion. We note that the untying time of a knot in an elongational field generally will not approach that of a knot held under constant tension as Wi tends to zero because the knot size and chain extension do not change appreciably as the knot diffuses off a uniformly tensioned chain. For a knot on a chain held at constant tension to fully untie, the knot has to diffuse the entirety of the distance between the knot boundary and chain end, while a knot in an elongational field at low Wi is aided in the process by a swelling knot and continuously decreasing chain extension. Nevertheless, the untying time of a knot held under constant tension is a useful upper bound for reference. That the untying time of a 5_1 knot approaches the upper bound at low Wi is likely due to the small knot size involved, which gives rise to a less dramatic change in extension during the untying process.

From Figure 7 (panels b−d), we observe that the knot untying times reach a diffusive limit at low Wi and a convective limit at high Wi, with the untying times for all knots approaching the lower convective bound at high Wi. Furthermore, the more complex the knot, the higher the Wi at which the diffusive and convective limits are reached. Specifically, the untying time for the 5_1 knot approaches the convective limit for $\mathrm{Wi} \geq 1.5$, whereas the untying time for the 10_1 knot does so only for $\mathrm{Wi} \geq 3$. Similarly, the untying time for the 10_1 knot evidently approaches a diffusive limit for $\mathrm{Wi} \leq 1.25$, while the untying time for the 5_1 knot does so at $\mathrm{Wi} \leq 0.6$. At a given Wi, more complex or larger knots result in a lower $\mathrm{Wi}_{\mathrm{eff}}$, thus the chain is in a less elongated state. The closer the molecule is to a coiled conformation, the more likely for the knot to move along the chain in a diffusive manner (Figures 3a and 5a). Conversely, smaller knots lead to a higher $\mathrm{Wi}_{\mathrm{eff}}$ and a more stretched conformation. Although the knot untying process is initiated by a knot being convected off the chain, because of the change in knot size and consequent change in chain extension as the knot unties, the untying process can be diffusion- or convection-driven. See the Supporting Information for distributions of untying times and plot of coefficient of variation for untying times as a function of Wi.

4. DISCUSSION

Given that knots are capable of affecting polymer properties,[31,34,48,59] there has been growing interest in studying not only the knotting dynamics of polymers but also the unknotting dynamics of chains with free ends. Practically, because knots can reduce the accuracy of next-generation genomics technologies, such as nanochannel genome mapping that relies on uniform stretching of molecules to convert physical distances between markers to genomic distances,[43−45] the process of untying knots is relevant for the development of devices that precondition DNA for such applications.

This work delves into the process of untying knots in elongational fields. The varying tension along a polymer chain in an elongational field leads to a dynamic change in knot size as the knot is convected off the chain by the field. Specifically, because tension at the ends of the chain tends to zero, the knot swells as it moves off the chain. This, in turn, gives rise to a change in $\mathrm{Wi}_{\mathrm{eff}}$, consequently causing untying-induced changes in chain conformation, the extent of which depends on knot complexity and field strength. For large knots and low Wi, the resulting knot size might be sufficient to bring the molecule through the coil−stretch transition as the knot unties, which brings about large changes in chain conformation during the untying process. We note that our simulation results are independent of the DNA model used and can be generalized to long polymer chains in elongational fields.

It is important to note that flow kinematics strongly influence the knot untying process. As an example, consider knots on polymers confined in nanochannels, which behave similarly to knots along tensioned chains. Due to uniform tension along the chain, the knot size remains relatively constant as the knot moves off the chain and the chain does not undergo appreciable changes in extension as the knot unties.[25,60] The dramatic chain conformational changes observed for the knot untying process in elongational fields is a consequence of the varying tension along a chain coupled with the existence of a coil−stretch transition.

Elongational and shear flows are the simplest flow types and hence most commonly studied. A computational study on the dynamics of flexible fibers in steady shear flow found that the flow is capable of knotting and unknotting a 3_1 knot.[61] Although the untying of complex knots in shear flows has not yet been investigated, we can hypothesize what would be observed. The complete untying of a complex knot typically occurs over multiple untying events, with each event requiring a chain end to be pulled through the knot. As shown in the current and previous studies,[33,37] the extensional character of elongational fields serves to convect knots off chains. In simple shear flow, for which the extensional and rotational components have equal magnitudes, the rotational component of the flow causes molecules to undergo end-over-end tumbling motion and thus large fluctuations in chain extension.[62,63] We expect the stochastic tumbling motion of a knotted polymer in shear flow to prevent the knot from reaching a chain end and frustrate the complete untying of a complex knot. Furthermore, since the rate of extension fluctuations increases with shear rate,[62] we postulate that knots will be longer-lived in flows with higher shear rates, in contrast to the decrease in untying time with increasing strain rate observed in elongational fields. Due to the large fluctuations in chain extension and lack of a sharp coil−stretch transition,[62] we believe that the untying-induced change in extension seen in elongational fields will not be apparent in shear flows.

It is worth noting that unknotting-knotting transitions in linear polymers, meaning spontaneous tying of a knot following an untying event, have been reported at equilibrium,[24] in nanochannels,[25,26] and in steady shear flow.[61] Such transitions in

DOI: 10.1021/acs.macromol.8b01879
Macromolecules 2018, 51, 9562−9571

equilibirum and in nanochannels reflect the equilibrium incidence of knots for given geometric constraints.[24−26] The existence of such transitions in simple shear flow, on the other hand, indicates that shear flow is capable of tying knots on molecules.[61] Given that elongational fields serve to convect knots off chains,[33,37] it is unsurprising that we do not observe the spontaneous formation of knots on molecules in elongational fields. Even if unknotting-knotting transitions do exist in elongational fields, we believe the effects to be fleeting and have an insignificant impact on overall untying dynamics. Since spontanoeus knot formation is absent in elongational fields, it is convenient to use such conditions for the study of knot untying processes.

5. CONCLUSION

In this work, we have used Brownian dynamics simulations and single-molecule DNA experiments to systematically study the untying process of knotted chains in elongational fields. Both simulation and experimental results show that the change in knot size during the knot untying process leads to a change in Wi_{eff}, which in turn causes a change in chain extension. The larger the knot and the lower the Wi, the more dramatic the transient changes in chain conformation. In some cases, the knot is large enough to induce a stretch-coil transition as the knot convects off the chain, followed by a coil−stretch transition as the knot partially unties. We investigated two metrics defined for the untying process: change in chain extension induced by knot untying and untying time. On the basis of a scaling analysis and empirical results, we showed that simulations predict a quadratic relationship between the change in extension due to knot untying and initial knot size for $Wi \geq 1.5$. Even though the knot untying process is initiated by convection of a knot off the chain, because of the change in knot size as the knot moves along the chain that leads to a change in chain extension as a knot unties, the untying process can be dominated by diffusion (low Wi or large knot) or convection (high Wi or small knot).

Given the ubiquity of knots in long polymers of both natural and synthetic origin, it is important to understand how the rheological properties of polymers is impacted not only by the presence of knots but also by the removal of knots. This study has shown that knotted molecules in elongational fields can undergo large, transient conformational changes as a knot moves off the chain and unties. Looking forward, we hope that our work will motivate further mechanistic studies into the unknotting of polymer chains, such as the untying of knots in other flows or fields and the untying pathways of knots.

■ ASSOCIATED CONTENT

Supporting Information

The Supporting Information is available free of charge on the ACS Publications website at DOI: 10.1021/acs.macromol.8b01879.

Detailed experimental method, simulation movies details, schematics of simulated knot types, individual simulation trajectories in elongational fields and at constant tension, further analysis of Δr_{max}, distribution of untying times and calculation of confidence intervals (PDF)

Simulation movies (ZIP)

■ AUTHOR INFORMATION

Corresponding Author

*E-mail: pdoyle@mit.edu.

ORCID

Beatrice W. Soh: 0000-0001-8399-5995

Alexander R. Klotz: 0000-0002-1581-6956

Patrick S. Doyle: 0000-0003-2147-9172

Notes

The authors declare no competing financial interest.

■ ACKNOWLEDGMENTS

This work was supported by the Singapore-MIT Alliance for Research and Technology (SMART) and National Science Foundation (NSF) Grant CBET-1602406. B.W.S. is funded by the Agency for Science, Technology and Research (A*STAR), Singapore.

■ REFERENCES

(1) Liu, L. F.; Perkocha, L.; Calendar, R.; Wang, J. C. Knotted DNA from bacteriophage capsids. *Proc. Natl. Acad. Sci. U. S. A.* **1981**, *78* (9), 5498−502.

(2) Arsuaga, J.; Vázquez, M.; Trigueros, S.; Sumners, D. W.; Roca, J. Knotting probability of DNA molecules confined in restricted volumes: DNA knotting in phage capsids. *Proc. Natl. Acad. Sci. U. S. A.* **2002**, *99* (8), 5373−5377.

(3) Nureki, O.; Shirouzu, M.; Hashimoto, K.; Ishitani, R.; Terada, T.; Tamakoshi, M.; Oshima, T.; Chijimatsu, M.; Takio, K.; Vassylyev, D. G.; Shibata, T.; Inoue, Y.; Kuramitsu, S.; Yokoyama, S. An enzyme with a deep trefoil knot for the active-site architecture. *Acta Crystallogr., Sect. D: Biol. Crystallogr.* **2002**, *58*, 1129−1137.

(4) Virnau, P.; Mirny, L. A.; Kardar, M. Intricate Knots in Proteins: Function and Evolution. *PLoS Comput. Biol.* **2006**, *2* (9), 1074−1079.

(5) Sumners, D. W.; Whittington, S. G. Knots in self-avoiding walks. *J. Phys. A: Math. Gen.* **1988**, *21* (7), 1689−1694.

(6) Frank-Kamenetskii, M. D.; Lukashin, A. V.; Vologodskii, A. V. Statistical mechanics and topology of polymer chains. *Nature* **1975**, *258* (5534), 398−402.

(7) Michels, J P J.; Wiegel, F. W. Probability of Knots in a Polymer Ring. *Phys. Lett. A* **1982**, *90* (7), 381−384.

(8) Dai, L.; van der Maarel, J. R. C.; Doyle, P. S. Effect of Nanoslit Confinement on the Knotting Probability of Circular DNA. *ACS Macro Lett.* **2012**, *1* (6), 732−736.

(9) Shaw, S.; Wang, J. Knotting of a DNA Chain During Ring Closure. *Science* **1993**, *260*, 533−536.

(10) Rybenkov, V. V.; Cozzarelli, N. R.; Vologodskii, A. V. Probability of DNA knotting and the effective diameter of the DNA double helix. *Proc. Natl. Acad. Sci. U. S. A.* **1993**, *90* (11), 5307−5311.

(11) Orlandini, E.; Whittington, S. G. Statistical topology of closed curves: Some applications in polymer physics. *Rev. Mod. Phys.* **2007**, *79* (2), 611−642.

(12) Grosberg, A. Y. A few notes about polymer knots. *Polym. Sci., Ser. A* **2009**, *51* (1), 70−79.

(13) Virnau, P.; Kantor, Y.; Kardar, M. Knots in Globule and Coil Phases of a Model Polyethylene. *J. Am. Chem. Soc.* **2005**, *127* (43), 15102−15106.

(14) Tubiana, L.; Orlandini, E.; Micheletti, C. Probing the Entanglement and Locating Knots in Ring Polymers: A Comparative Study of Different Arc Closure Schemes. *Prog. Theor. Phys. Suppl.* **2011**, *191*, 192−204.

(15) Grosberg, A. Y.; Rabin, Y. Metastable tight knots in a worm-like polymer. *Phys. Rev. Lett.* **2007**, *99*, 217801.

(16) Dobay, A.; Dubochet, J.; Millett, K.; Sottas, P.-E.; Stasiak, A. Scaling behavior of random knots. *Proc. Natl. Acad. Sci. U. S. A.* **2003**, *100* (10), 5611−5615.

(17) Huang, L.; Makarov, D. E. Translocation of a knotted polypeptide through a pore. *J. Chem. Phys.* **2008**, *129* (12), 121107.

(18) Rosa, A.; Di Ventra, M.; Micheletti, C. Topological Jamming of Spontaneously Knotted Polyelectrolyte Chains Driven Through a Nanopore. *Phys. Rev. Lett.* **2012**, *109* (11), 118301.

DOI: 10.1021/acs.macromol.8b01879
Macromolecules 2018, 51, 9562−9571

(19) Suma, A.; Rosa, A.; Micheletti, C. Pore Translocation of Knotted Polymer Chains: How Friction Depends on Knot Complexity. *ACS Macro Lett.* **2015**, *4* (12), 1420−1424.
(20) Plesa, C.; Verschueren, D.; Pud, S.; van der Torre, J.; Ruitenberg, J. W.; Witteveen, M. J.; Jonsson, M. P.; Grosberg, A. Y.; Rabin, Y.; Dekker, C. Direct observation of DNA knots using a solid-state nanopore. *Nat. Nanotechnol.* **2016**, *11* (12), 1093−1097.
(21) Narsimhan, V.; Renner, C. B.; Doyle, P. S. Translocation dynamics of knotted polymers under a constant or periodic external field. *Soft Matter* **2016**, *12* (22), 5041−5049.
(22) MoÌĹbius, W.; Frey, E.; Gerland, U. Spontaneous Unknotting of a Polymer Confined in a Nanochannel. *Nano Lett.* **2008**, *8* (12), 4518−4522.
(23) Raymer, D. M.; Smith, D. E. Spontaneous knotting of an agitated string. *Proc. Natl. Acad. Sci. U. S. A.* **2007**, *104* (42), 16432−16437.
(24) Tubiana, L.; Rosa, A.; Fragiacomo, F.; Micheletti, C. Spontaneous Knotting and Unknotting of Flexible Linear Polymers: Equilibrium and Kinetic Aspects. *Macromolecules* **2013**, *46* (9), 3669−3678.
(25) Micheletti, C.; Orlandini, E. Knotting and Unknotting Dynamics of DNA Strands in Nanochannels. *ACS Macro Lett.* **2014**, *3*, 876.
(26) Suma, A.; Orlandini, E.; Micheletti, C. Knotting dynamics of DNA chains of different length confined in nanochannels. *J. Phys.: Condens. Matter* **2015**, *27* (35), 354102.
(27) Bao, X. R.; Lee, H. J.; Quake, S. R. Behavior of Complex Knots in Single DNA Molecules. *Phys. Rev. Lett.* **2003**, *91* (26), 265506.
(28) Amin, S.; Khorshid, A.; Zeng, L.; Zimny, P.; Reisner, W. A nanofluidic knot factory based on compression of single DNA in nanochannels. *Nat. Commun.* **2018**, *9* (1), 1506.
(29) Tang, J.; Du, N.; Doyle, P. S. Compression and self-entanglement of single DNA molecules under uniform electric field. *Proc. Natl. Acad. Sci. U. S. A.* **2011**, *108* (39), 16153−16158.
(30) Zhou, C.; Reisner, W. W.; Staunton, R. J.; Ashan, A.; Austin, R. H.; Riehn, R. Collapse of DNA in AC Electric Fields. *Phys. Rev. Lett.* **2011**, *106* (24), 248103.
(31) Renner, C. B.; Doyle, P. S. Stretching self-entangled DNA molecules in elongational fields. *Soft Matter* **2015**, *11* (16), 3105−3114.
(32) Klotz, A. R.; Narsimhan, V.; Soh, B. W.; Doyle, P. S. Dynamics of DNA Knots during Chain Relaxation. *Macromolecules* **2017**, *50* (10), 4074−4082.
(33) Klotz, A. R.; Soh, B. W.; Doyle, P. S. Motion of Knots in DNA Stretched by Elongational Fields. *Phys. Rev. Lett.* **2018**, *120*, 188003.
(34) Soh, B. W.; Narsimhan, V.; Klotz, A. R.; Doyle, P. S. Knots modify the coil-stretch transition in linear DNA polymers. *Soft Matter* **2018**, *14*, 1689−1698.
(35) Vologodskii, A. Brownian dynamics simulation of knot diffusion along a stretched DNA molecule. *Biophys. J.* **2006**, *90* (5), 1594−1597.
(36) Huang, L.; Makarov, D. E. Langevin Dynamics Simulations of the Diffusion of Molecular Knots in Tensioned Polymer Chains. *J. Phys. Chem. A* **2007**, *111* (41), 10338−10344.
(37) Renner, C. B.; Doyle, P. S. Untying Knotted DNA with Elongational Flows. *ACS Macro Lett.* **2014**, *3*, 963−967.
(38) Saitta, A. M.; Soper, P. D.; Wasserman, E.; Klein, M. L. Influence of a knot on the strength of a polymer strand. *Nature* **1999**, *399*, 46−48.
(39) de Gennes, P. G. Reptation of a Polymer Chain in the Presence of Fixed Obstacles. *J. Chem. Phys.* **1971**, *55* (2), 572−579.
(40) Klein, J. Evidence for reptation in an entangled polymer melt. *Nature* **1978**, *271* (5641), 143−145.
(41) Kremer, K.; Grest, G. S. Dynamics of entangled linear polymer melts: A molecular dynamics simulation. *J. Chem. Phys.* **1990**, *92* (8), 5057−5086.
(42) Qin, J.; Milner, S. T. Counting polymer knots to find the entanglement length. *Soft Matter* **2011**, *7*, 10676−10693.
(43) Lam, E. T.; Hastie, A.; Lin, C.; Ehrlich, D.; Das, S. K.; Austin, M. D.; Deshpande, P.; Cao, H.; Nagarajan, N.; Xiao, M.; Kwok, P.-Y. Genome mapping on nanochannel arrays for structural variation analysis and sequence assembly. *Nat. Biotechnol.* **2012**, *30* (8), 771−776.
(44) Reisner, W.; Pedersen, J. N.; Austin, R. H. DNA confinement in nanochannels: physics and biological applications. *Rep. Prog. Phys.* **2012**, *75* (10), 106601.
(45) Dorfman, K. D.; King, S. B.; Olson, D. W.; Thomas, J. D. P.; Tree, D. R. Beyond gel electrophoresis: microfluidic separations, fluorescence burst analysis, and DNA stretching. *Chem. Rev.* **2013**, *113* (4), 2584−667.
(46) de Gennes, P. G. Coil-stretch transition of dilute flexible polymers under ultrahigh velocity gradients. *J. Chem. Phys.* **1974**, *60* (12), 5030−5042.
(47) Perkins, T. T.; Smith, D. E.; Chu, S. Single Polymer Dynamics in an Elongational Flow. *Science* **1997**, *276* (5321), 2016−2021.
(48) Narsimhan, V.; Klotz, A. R.; Doyle, P. S. Steady-State and Transient Behavior of Knotted Chains in Extensional Fields. *ACS Macro Lett.* **2017**, *6* (11), 1285−1289.
(49) Allison, S. A. Brownian dynamics simulation of wormlike chains. Fluorescence depolarization and depolarized light scattering. *Macromolecules* **1986**, *19* (1), 118−124.
(50) Jian, H.; Vologodskii, A. V.; Schlick, T. A Combined Wormlike-Chain and Bead Model for Dynamic Simulations of Long Linear DNA. *J. Comput. Phys.* **1997**, *136* (1), 168−179.
(51) Klenin, K.; Merlitz, H.; Langowski, J. A Brownian Dynamics Program for the Simulation of Linear and Circular DNA and Other Wormlike Chain Polyelectrolytes. *Biophys. J.* **1998**, *74* (2), 780−788.
(52) Stigter, D. Interactions of highly charged colloidal cylinders with applications to double-stranded DNA. *Biopolymers* **1977**, *16* (7), 1435−1448.
(53) Huang, J.; Schlick, T.; Vologodskii, A. Dynamics of site juxtaposition in supercoiled DNA. *Proc. Natl. Acad. Sci. U. S. A.* **2001**, *98* (3), 968−73.
(54) Liu, T. W. Flexible polymer chain dynamics and rheological properties in steady flows. *J. Chem. Phys.* **1989**, *90* (10), 5826−5842.
(55) Somasi, M.; Khomami, B.; Woo, N. J.; Hur, J. S.; Shaqfeh, E. S. G. Brownian dynamics simulations of bead-rod and bead-spring chains: numerical algorithms and coarse-graining issues. *J. Non-Newtonian Fluid Mech.* **2002**, *108* (1−3), 227−255.
(56) Vologodskii, A. V.; Lukashin, A. V.; Frank-Kamenetskii, M. D.; Anshelevich, V. V. The knot problem in statistical mechanics of polymer chains. *Journal of Experimental and Theoretical Physics* **1974**, *66*, 2153−2163.
(57) Narsimhan, V.; Renner, C. B.; Doyle, P. S. Jamming of Knots along a Tensioned Chain. *ACS Macro Lett.* **2016**, *5* (1), 123−127.
(58) Clisby, N. Accurate Estimate of the Critical Exponent ν for Self-Avoiding Walks via a Fast Implementation of the Pivot Algorithm. *Phys. Rev. Lett.* **2010**, *104* (5), 055702.
(59) Caraglio, M.; Micheletti, C.; Orlandini, E. Stretching Response of Knotted and Unknotted Polymer Chains. *Phys. Rev. Lett.* **2015**, *115* (18), 188301.
(60) Metzler, R.; Reisner, W.; Riehn, R.; Austin, R.; Tegenfeldt, J. O.; Sokolov, I. M. Diffusion mechanisms of localised knots along a polymer. *Europhys. Lett.* **2006**, *76* (4), 696−702.
(61) Kuei, S.; Słowicka, A. M.; Ekiel-Jeżewska, M. L.; Wajnryb, E.; Stone, H. A. Dynamics and topology of a flexible chain: knots in steady shear flow. *New J. Phys.* **2015**, *17* (5), 053009.
(62) Smith, D. E.; Babcock, H. P.; Chu, S. Single-polymer dynamics in steady shear flow. *Science* **1999**, *283* (5408), 1724−7.
(63) Schroeder, C. M.; Teixeira, R. E.; Shaqfeh, E. S. G.; Chu, S. Dynamics of DNA in the Flow-Gradient Plane of Steady Shear Flow: Observations and Simulations. *Macromolecules* **2005**, *38* (5), 1967−1978.

DOI: 10.1021/acs.macromol.8b01879
Macromolecules 2018, 51, 9562−9571